Coulomb-interaction induced coupling of Landau levels in intrinsic and modulation-doped quantum wells

J. Paul,[1] C. E. Stevens,[1] H. Zhang,[1] P. Dey,[1] D. McGinty,[1] S. A. McGill,[2] R. P. Smith,[3] J. L. Reno,[4] V. Turkowski,[5] I. E. Perakis,[6] D. J. Hilton,[6] and D. Karaiskaj[1,*]

[1]*Department of Physics, University of South Florida, 4202 East Fowler Avenue, Tampa, Florida 33620, USA*
[2]*National High Magnetic Field Laboratory, Florida State University, Tallahassee, Florida 30201, USA*
[3]*Department of Physics, California State University, East Bay, Hayward, California 94542, USA*
[4]*CINT, Sandia National Laboratories, Albuquerque, New Mexico 87185, USA*
[5]*Department of Physics, University of Central Florida, Orlando, Florida 32816, USA*
[6]*Department of Physics, University of Alabama at Birmingham, Birmingham, Alabama 35294, USA*

(Received 11 November 2016; revised manuscript received 1 June 2017; published 28 June 2017)

We have performed two-dimensional Fourier transform spectroscopy on intrinsic and modulation doped quantum wells in external magnetic fields up to 10 T. In the undoped sample, the strong Coulomb interactions and the increasing separations of the electron and hole charge distributions with increasing magnetic fields lead to a nontrivial in-plane dispersion of the magneto-excitons. Thus, the discrete and degenerate Landau levels are coupled to a continuum. The signature of this continuum is the emergence of elongated spectral line shapes at the Landau level energies, which are exposed by the multidimensional nature of our technique. Surprisingly, the elongation of the peaks is completely absent in the lowest Landau level spectra obtained from the modulation doped quantum well at high fields.

DOI: 10.1103/PhysRevB.95.245314

I. INTRODUCTION

In undoped or intrinsic quantum wells electrons can be promoted in the conduction band optically, leaving positively charged holes in the valence band. The Coulomb attraction between electrons and holes leads to bound quasiparticles called excitons [1]. These can further form higher four-particle bound quasiparticles called biexcitons [2]. Excitons show a quadratic diamagnetic shift in energy with the external field. At high magnetic fields Landau levels also form, which instead shift linearly in energy with the applied magnetic field, if valence band mixing is neglected [3–7].

The introduction of dopants in quantum wells moves the Fermi edge into the conduction band. The dopant atoms are placed in the barrier region of the quantum well, known as modulation doping or δ doping. In a strong magnetic field, the two-dimensional electrons in the doped system form Landau levels. At low temperatures, a correlated system is formed that exhibits unique electronic transport properties such as the integer and fractional quantum Hall effects [8]. The two-dimensional electron gas in semiconductor quantum systems is the subject of renewed interest as a result of the discovery of three-dimensional topological insulators [9]. The two-dimensional electron gas in the quantum Hall regime have been extensively studied using transport measurements. However, transport measurements probe only the conducting edge states, whereas optical methods have the ability to probe the Landau levels in the insulating bulk.

Light scattering and photoluminescence measurement in the quantum Hall regime and have provided important insights into the physics of optical excitations at high magnetic fields [10–22]. The light scattering experiments have lead to the observation of magnetorotons and have provided details into the physics of composite fermions at different fractional filling factors [23–30]. The time-resolved coherent spectroscopy provides unique tools to study the dynamics of strongly correlated systems. It can probe directly contributions that occur as a result of four-particle and higher terms in perturbation theory [31–41]. Recently, two-dimensional Fourier transform (2DFT) spectroscopy was developed, which can provide details of the may-body interactions that cannot be obtained using other methods. The correlated nature of the frequency axes can reveal underlying physics in the form of two-dimensional line shapes and additional peaks in the 2DFT frequency spectra [42–48].

In the present study, 2DFT spectroscopy reveals distinct differences in the Landau levels originating from undoped and modulation doped quantum wells. In the undoped sample elongated line shapes along the ω_τ frequency direction of the 2DFT spectra are observed [45,51,52]. This behavior was expected to be stronger in the modulation doped sample due to the higher probability of quasiparticle scattering with free carriers. Surprisingly, the elongated line shapes are completely absent in the lowest Landau level in the modulation doped quantum well sample between 8 and 10 T.

In order to understand this seemingly counterintuitive behavior, we perform time-dependent density functional theory (DFT) calculations [53–56]. Density matrix time-dependent DFT reveals the underlying physics and attributes the elongated line shapes to the effect of Coulomb interactions on the inhomogeneities within the electron and hole charge density overlap, which couples discrete Landau levels to a continuum state. In the time-dependent DFT formalism, these inhomogeneities are taken into account in the exchange-correlation potential. The electron and hole charge distributions become progressively separated with increasing magnetic fields, leading to an overlap of the charge densities which becomes comparable to the in-plane lattice constant. These charge inhomogeneities within the charge density overlap become

*karaiskaj@usf.edu

sufficiently important, leading to a breakdown on Kohn's theorem [57–59]. However, the absence of the elongated line shapes in the ω_τ direction of the 2DFT spectra in the doped sample is attributed to the effect of screening of the Coulomb interactions, which leads to a reduced effect of the inhomogeneity within the charge density overlap and restores Kohn's theorem.

Finally, in the undoped quantum well, strong quantum coherent coupling between the Landau levels is observed, leading to distinct cross-diagonal peaks in the two-dimensional spectra. Inter-Landau-level coherent coupling was first observed as a beating in the time-integrated four-wave mixing (FWM) signal [38,40]. However, time-integrated FWM cannot unambiguously distinguish between quantum coherence and polarization beating. The appearance of cross-peaks below and above the diagonal in 2DFT spectroscopy provides a clear indication of quantum coherence coupling [60].

II. EXPERIMENT AND SAMPLES

The experimental setup used in the present study is shown in Fig. 1. Three laser pulses are incident on the sample in directions $\vec{k}_a$, $\vec{k}_b$, and $\vec{k}_c$ and are separated by the time delays τ and T. The third-order nonlinear interaction gives rise to a signal in the direction $-\vec{k}_a + \vec{k}_b + \vec{k}_c$. By varying the time delay τ and monitoring the FWM intensity, referred as time integrated FWM, the dephasing time of excitons can be measured. In 2DFT spectroscopy, the time delays τ and t are monitored simultaneously while scanning with interferometric precision and accurately preserving the phase. The Fourier transform to the frequency domain with respect to the two time delays τ and t leads to correlated two-dimensional frequency spectra dependent on ω_τ and ω_t [61]. The extension to two frequency axes is not merely a more convenient way of plotting the data, since the axes are now correlated, analogous to the extension of nuclear magnetic resonance to two dimensions [62]. When the spectra are plotted with respect to $-\omega_\tau$ and ω_t the resonances probed appear along the diagonal, whereas signatures of quantum coherent coupling can be manifested as cross-diagonal peaks [60]. Furthermore, the two-dimensional line shapes are highly sensitive to the many-body interactions in the sample, making this technique very suited to study many-body effects. The advantages of multidimensional spectroscopy are well documented in the literature, where in semiconductor materials 2DFT spectroscopy has provided insights into the microscopic details of the many-body interactions [43,44].

The laser pulses with a duration ∼130 fs were generated by a standard tunable Ti:sapphire oscillator. The samples were held at 1.6 K inside the Oxford Spectromag magneto-optical cryostat. The magnetic field was applied in the Faraday geometry perpendicular to the sample surface and could be varied from zero up to 10 T. Two quantum well samples were used in the present studies, one undoped (intrinsic) with 12 nm well thickness and a modulation doped 18 nm GaAs/AlGaAs quantum well with in-well carrier concentration of $\sim 4 \times 10^{11}$ cm^{-2}. The samples were studied using different optical techniques and the carrier concentration has been unambiguously determined [47,63].

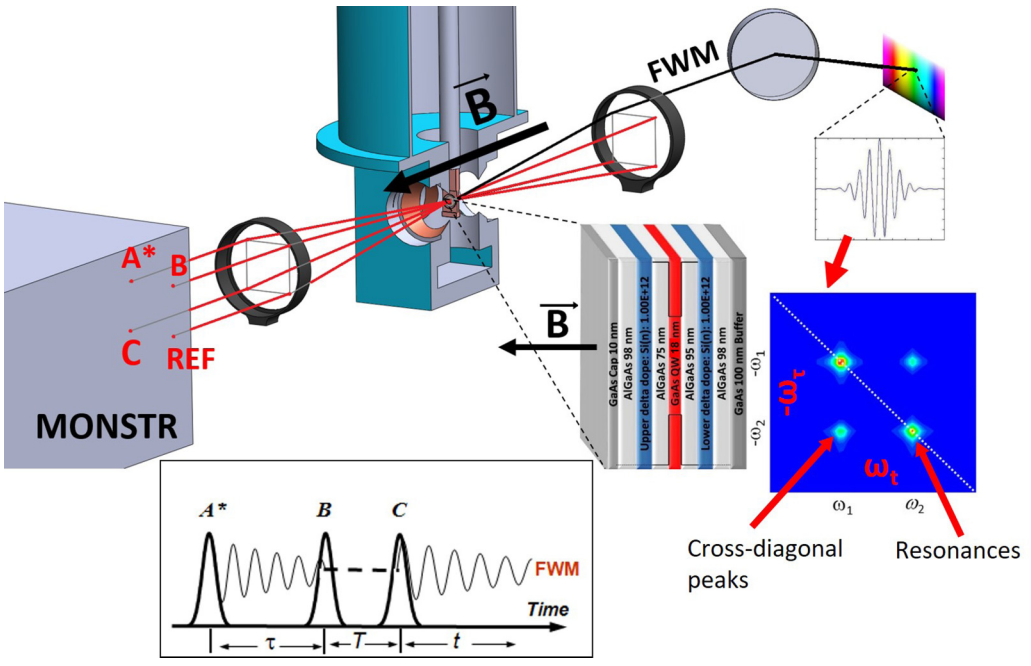

FIG. 1. Schematic of the experimental setup: The four phase-stabilized laser beams are provided by the MONSTR instrument [49,50]. Three beams labeled A*, B, and C are used to generate the FWM signal, where A* corresponds to the phase conjugate beam. The beams are aligned in the three corners of a square. The FWM signal generated at the sample propagates along the missing corner (direction $-\vec{k}_a + \vec{k}_b + \vec{k}_c$). A fourth beam labeled "Ref." is used to trace the FWM and as the local oscillator for heterodyne detection. The samples are kept at 1.6 K inside the magneto-optical cryostat. The magnetic fields up to 10 T are applied perpendicular to the sample surface in Faraday geometry. The FWM signal is heterodyne detected and dispersed into a spectrometer. The Fourier transformed spectral interferograms lead to the 2DFT spectra. (Sample ID: VA0607.)

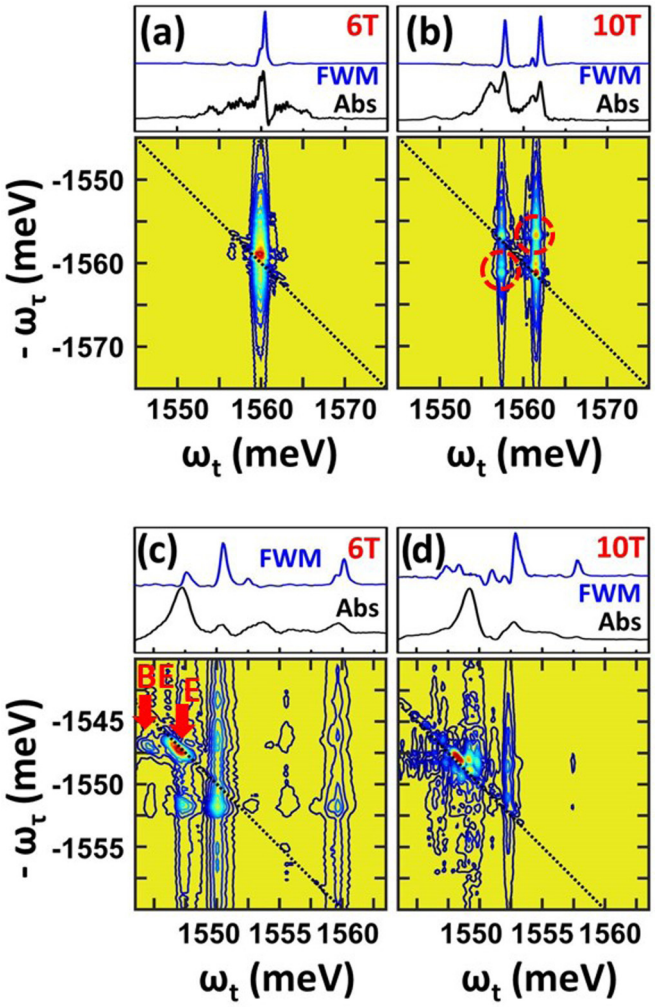

FIG. 2. Experimental S_I 2DFT spectra of the undoped GaAs quantum well at (H,H,H,H) linear horizontal polarizations under high magnetic fields. The linear horizontal (H,H,H,H) polarizations correspond to A*, B, C, and detection, respectively. The spectrally resolved FWM (blue line) and the absorbance (black line) are shown above the experimental spectra. Upper row: 2DFT spectra of the Landau levels from the undoped GaAs quantum well at magnetic fields of (a) 6 T and (b) 10 T. Bottom row: 2DFT spectra of the excitonic region from the undoped GaAs quantum well at magnetic fields of (c) 6 T and (d) 10 T.

III. RESULTS

We start our discussion with the intrinsic GaAs quantum wells, where the exciton ground state is strongly bound due to Coulomb interactions. Several excited states of the exciton are observed, which shift linearly with magnetic fields. The level assignment of the excited states has been discussed in the literature and is not the subject of the present study [3,4,64–69]. The laser pulses generated by the oscillator, with a full width at half maximum of ∼15 meV, were tuned resonantly with these Landau levels. Therefore, only the spectral range excited by the laser pulse can be observed. In Figs. 2(a) and 2(b) 2DFT spectra of Landau levels originating from the undoped quantum well are shown at 6 and 10 T. The two-dimensional Landau level spectra show full widths at half maximum below 1 meV along the ω_t frequency in the 2DFT spectra, but much larger and elongated line shapes along the ω_τ frequency [45,51,52,61]. Furthermore, the two Landau levels shown at 10 T reveal strong quantum coherent coupling between them, as indicated by the cross-diagonal peaks marked by the red dashed circles [70,71].

The 2DFT spectra in the frequency region of the excitonic ground state are shown in Figs. 2(c) and 2(d) at 6 and 10 T, respectively. It should be noted here that the excitonic ground state, which shows a diamagnetic quadratic shift with magnetic fields, lies at lower energies than the Landau levels shown in Figs. 2(a) and 2(b). Therefore, the center wavelength of the laser has been tuned towards lower energies and only the spectral range excited by the laser can be observed. At 6 T both the exciton and biexciton peaks can be observed in Fig. 2(c) and are marked by the red arrows. As previously shown, the exciton and biexciton resonances do not show the vertical elongation along the ω_τ frequency, but are slightly elongated along the diagonal of the 2DFT spectra due to inhomogeneous broadening [60]. This further confirms the preservation of the phase stability during the 2DFT measurements.

Such peculiar elongated line shapes along the ω_τ observed for the Landau levels have in the past been observed in the absence of magnetic fields and have been attributed to interactions with the continuum [47,51,52]. However, in the present high quality sample the discrete nature of the Landau levels and the quantum confinement of the quantum well in the magnetic field direction should not lead to such continuum state interactions. According to Kohn's theorem the Coulomb interaction should not lead to an in-plane dispersion of charge excitations and alter the frequency of the Landau levels [57,72–74]. In contrast, along the ω_t frequency direction the Landau levels remain narrow with increasing fields. This is further observed in the much narrower spectrally resolved FWM spectra as compared to the absorption spectra in Fig. 2.

We further proceed by discussing the modulation doped quantum well. The absorption spectra are shown in Fig. 3(a) and follow patterns reported previously in the literature [35]. With increasing magnetic fields the formation of Landau levels can be observed, starting with LL1. Between 4 and 5 T only LL1 is populated and shifts toward higher energy with increasing magnetic field. At higher magnetic fields starting at 8 T, only the lowest Landau level LL0 is populated [70,71]. The polarization dependence of LL1 and LL0 is shown in Figs. 3(b) and 3(c) for circular σ^+ and σ^- polarizations. The first Landau level LL1 shows only a small energy shift between the σ^+ and σ^- polarizations, whereas the lowest Landau level LL0 is strongly polarization dependent. The lowest Landau energy level at fixed momentum accommodates only particles with one projection of spin, while the next level is filled with particles with both spins [75]. This likely leads to the strong polarization dependence of the lowest Landau level.

The time-integrated FWM was measured for LL1 and LL0 at 6.5 and 10 T, respectively and results are shown in Fig. 3(d). A rapid dephasing of several hundred femtoseconds is observed for both Landau levels. The fast dephasing is followed by a much slower component, lasting several picoseconds. The longer decay component is measured at 4.6 ps for LL1 and increases further to 6.2 ps for LL0. The longer dephasing for LL0 is likely due to underpopulation of the level as compared to LL1, and hence reduced scattering

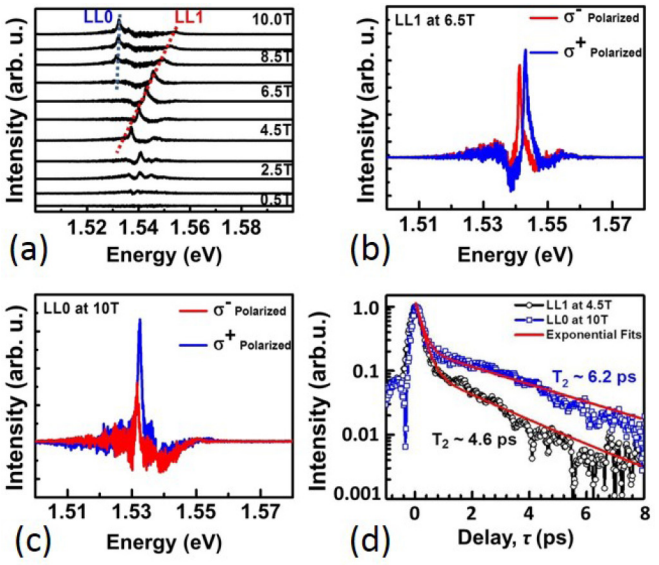

FIG. 3. (a) Absorbance of the modulation doped GaAs quantum well showing the two lowest Landau levels LL0 and LL1 at different magnetic field strengths from 0 to 10 T. Both Landau levels shift linearly with temperature, marked by the dashed lines. (b) Polarization dependent absorption spectra of the LL1 at 6.5 T. (c) Polarization dependent absorption spectra of the LL0 at 10 T. (d) Time-integrated FWM of the LL1 at 4.5 T (black squares) and LL0 at 10 T (blue squares). The red lines are the exponential fittings.

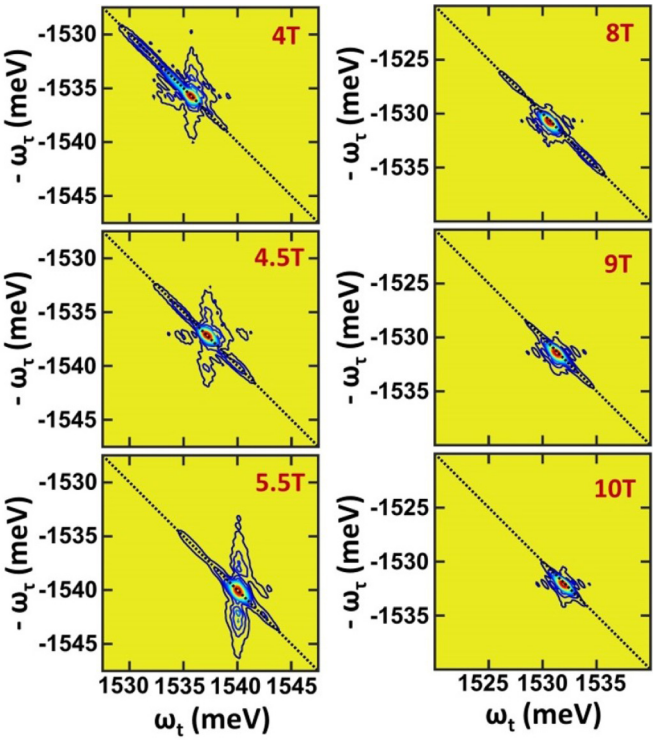

FIG. 4. Left: Experimental S_I 2DFT spectra using $(\sigma^+\sigma^+\sigma^+\sigma^+)$ polarizations of LL1 at three different magnetic fields (4, 4.5, and 5.5 T). Right: Experimental S_I 2DFT spectra using $(\sigma^+\sigma^+\sigma^+\sigma^+)$ polarizations of LL0 at three different magnetic fields (8, 9, and 10 T).

effects. On the other hand, the initial ∼100 fs relaxation for both levels is due to similar ultrafast preequilibration of the quasifree excitations.

The 2DFT spectra for the modulation doped quantum well are shown in Fig. 4 for LL1 (left) and LL0 (right) at three different magnetic fields. Surprisingly, the elongation in the ω_τ frequency direction of the transitions observed in the undoped quantum well is substantially reduced for LL1, and is completely absent for LL0. Despite the much higher concentration of the free carriers in the modulation doped sample, there is no stripe-like elongation for the lowest Landau level at fields between 8 and 10 T.

IV. DISCUSSION

In order to gain a deeper understanding of the physics behind the behavior of the Landau levels in doped and undoped quantum wells, we performed density matrix time-dependent DFT calculations for both samples, which are shown in Fig. 5. The details of the time-dependent DFT calculations are provided in recently published articles [53–56] and in Ref. [76]. The theory reproduces well the elongated line shapes of the Landau levels in the undoped sample in Figs. 5(a) and 5(b). Furthermore, at lower energies the theoretical calculations replicate the bound exciton and biexciton peaks in the 2DFT spectra [Figs. 5(c) and 5(d)]. Although not as well resolved, the cross-peaks due to quantum coherent coupling are shown in Fig. 5(b) and are marked by the red circles.

The time-dependent DFT calculations reveal the underlying physics and attribute the elongated line shapes to breaking of the translational invariance by inhomogeneities in the exchange-correlation potential. The inhomogeneity effects become important when the characteristic field-related length scales, i.e., the overlap of the electron-hole wave functions, becomes comparable to or smaller than the in-plane lattice constant. The calculated spatial charge density distribution is shown in Fig. 6, where the blue and green circles estimate the effective sizes of the electron and hole clouds. The red arrow shows the effective distance between the electron and hole charge densities. The overlap between electron and hole charge densities decreases with increasing magnetic fields, approaching the in-plane lattice constant for higher fields. The unscreened Coulomb interactions in the undoped sample have a stronger effect on the charge inhomogeneities within the charge density overlap, bringing the system outside the Kohn's theorem protective limits. Thus, the highly degenerate and discrete Landau levels couple coherently forming a continuum, revealed by the elongated line shapes. Anomalies beyond Kohn's theorem have been observed in the past and were caused by phonons, nonparabolic electron dispersion, and Coulomb interactions [58,59,77–79].

The excitonic response of semiconductors is described by the optical polarization [2]. We obtain the optical polarization $P(\omega)$ using the density-matrix time-dependent DFT equation, which has the following form:

$$\sum_{\mathbf{k}'}\left[\left(\epsilon^{c}_{\mathbf{k}+\mathbf{q}}-\epsilon^{v}_{\mathbf{k}}\right)\delta_{\mathbf{k}\mathbf{k}'}+F^{cvvc}_{\mathbf{k}\mathbf{k}\mathbf{k}'\mathbf{k}'}\right]P_{\mathbf{k}'+\mu\mathbf{q}}(\omega)=\omega P_{\mathbf{k}+\mu\mathbf{q}}(\omega), \tag{1}$$

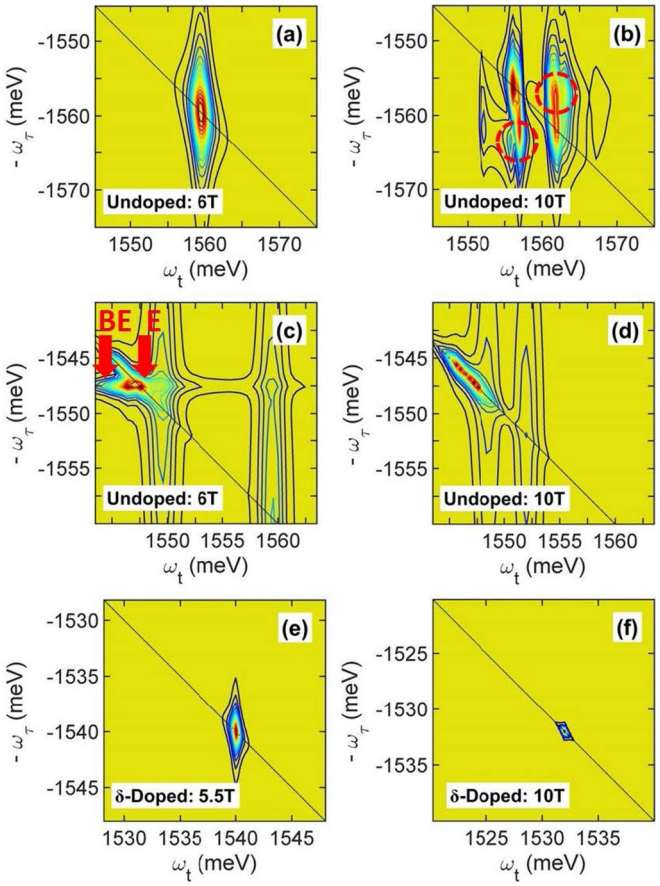

FIG. 5. Theoretical S_I 2DFT spectra of the undoped GaAs quantum well under high magnetic fields, calculated using time-dependent DFT. 2DFT spectra of the Landau levels from the undoped GaAs quantum well at magnetic fields of (a) 6 T and (b) 10 T. 2DFT spectra of the excitonic spectral region from the undoped GaAs quantum well at magnetic fields of (c) 6 T and (d) 10 T. Theoretical S_I 2DFT spectra from the modulation doped sample. S_I 2DFT spectra of LL1 (e) at 5.5 T and LL0 (f) at 10 T, calculated using time dependent DFT.

where $\mathbf{q}$ is the exciton momentum, μ is the reduced pair mass, and $\epsilon^c_{\mathbf{k}}$ and $\epsilon^v_{\mathbf{k}}$ are the dispersions of the conduction and of the valence bands. In the doped case, there is an additional term in the left-hand side of the equation $\sum_{\mathbf{k}\mathbf{k}'} w^{cccc}_{\mathbf{k}\mathbf{k}\mathbf{k}'\mathbf{k}'} P_{\mathbf{k}'+\mu\mathbf{q}}(\omega)$, which describes the electron-electron repulsion potential defined by

$$w^{abcd}_{\mathbf{k}\mathbf{q}\mathbf{k}'\mathbf{q}'} = \frac{1}{\epsilon_{ee}} \int d\mathbf{r}_1 d\mathbf{r}_2 \psi^{a*}_{\mathbf{k}}(\mathbf{r}_1)\psi^{b}_{\mathbf{q}}(\mathbf{r}_1) \times \frac{1}{|\mathbf{r}_1-\mathbf{r}_2|}\psi^{c*}_{\mathbf{k}'}(\mathbf{r}_2)\psi^{d}_{\mathbf{q}'}(\mathbf{r}_2), \quad (2)$$

where ϵ_{ee} is the static dielectric screening. This term leads to screening of the attractive electron-hole interactions. In the time domain the effective electron-hole interactions are given by

$$F^{abcd}_{\mathbf{k}\mathbf{q}\mathbf{k}'\mathbf{q}'}(t_1,t_2) = \int d\mathbf{r}_1 \mathbf{r}_2 \phi^{a*}_{\mathbf{k}}(\mathbf{r}_1)\phi^{b}_{\mathbf{q}}(\mathbf{r}_1) \times f_{XC}(\mathbf{r}_1,t_1,\mathbf{r}_2,t_2)\phi^{c*}_{\mathbf{k}'}(\mathbf{r}_2)\phi^{d}_{\mathbf{q}'}(\mathbf{r}_2), \quad (3)$$

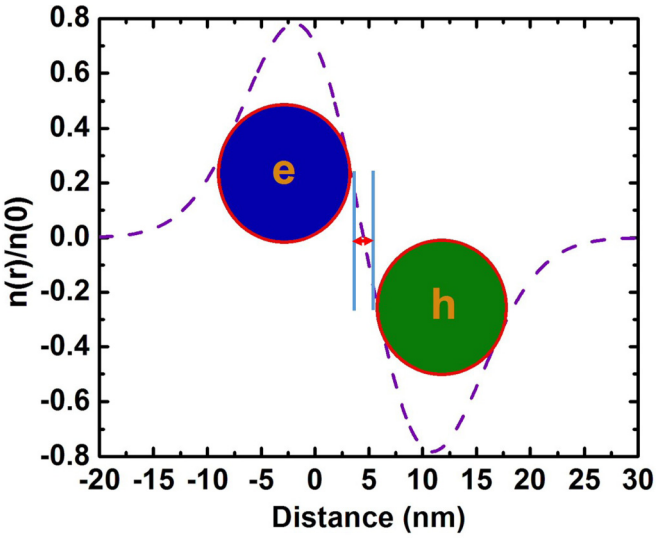

FIG. 6. The difference between the electron and hole charges at $B = 10$ T. The blue and green circles estimate the effective sizes of the electron and hole clouds (full width at half maximum). The red arrow shows effective distance between the electron and hole clouds. The opposite sign of the wave functions leads to a charge density in the area between the circles that is much smaller than the average individual electron and hole charge densities.

where $\phi^a_{\mathbf{k}}(\mathbf{r})$ are the static Kohn-Sham wave functions for the band a and momentum $\mathbf{k}$, obtained from the solution of static DFT equations. The matrix $F^{abcd}_{\mathbf{k}\mathbf{q}\mathbf{k}'\mathbf{q}'}(t_1,t_2)$ depends on the exchange-correlation kernel and therefore describes the strengths of the electron-hole attractions. In this article, we use the screened Slater expression for the exchange-correlation kernel kernel:

$$f_{XC}(\mathbf{r},t,\mathbf{r}'t') = -\delta(t-t')\frac{2\left|\sum_{j,\mathbf{k}}\phi^{j}_{\mathbf{k}}(\mathbf{r})\phi^{j*}_{\mathbf{k}}(\mathbf{r}')\right|^2}{\epsilon|\mathbf{r}-\mathbf{r}'|n_0(\mathbf{r})n_0(\mathbf{r}')}. \quad (4)$$

The spatial dependence of the equilibrium charge density $n_0(\mathbf{r})$ over the unit cell becomes significant in the regime of high magnetic fields and unscreened electron-hole interactions. In the time-dependent DFT calculations this becomes apparent when analyzing the expression for effective electron-hole scattering matrix in real space, $F(\mathbf{r},\mathbf{r}') = \iint e^{-i\mathbf{k}\mathbf{r}} F^{cvvc}_{\mathbf{k}\mathbf{k}\mathbf{k}'\mathbf{k}'}(\omega) e^{i\mathbf{k}'\mathbf{r}'} d^2\mathbf{k}\, d^2\mathbf{k}'$, which contains the exchange-correlation kernel f_{XC} [76]. Introducing the average and relative coordinate of the electron-hole pair, $\mathbf{R} = (\mathbf{r}+\mathbf{r}')/2$ and $\rho = \mathbf{r}-\mathbf{r}'$, one obtains

$$F(\mathbf{R},\rho) = \iint e^{-i(\mathbf{k}-\mathbf{k}')R} F^{cvvc}_{\mathbf{k}\mathbf{k}\mathbf{k}'\mathbf{k}'}(\omega) e^{i\frac{(\mathbf{k}+\mathbf{k}')}{2}\rho} d^2\mathbf{k}\, d^2\mathbf{k}'. \quad (5)$$

If the function $F^{cvvc}_{\mathbf{k}\mathbf{k}\mathbf{k}'\mathbf{k}'}(\omega)$ would depend on the difference of the momenta $\mathbf{q} = \mathbf{k}-\mathbf{k}'$, the standard translation invariant theory is obtained, leading to $F(\mathbf{R}) \sim \int d^2\mathbf{q}\, e^{-i\mathbf{q}\mathbf{R}} F^{cvvc}_{\mathbf{q}}(\omega)$. However, the lack of translational invariance, due to the spatial inhomogeneity within the reduced overlap of the charge density distributions, makes the interaction potential dependent on both coordinates $F(\mathbf{R},\rho)$, leading to a nontrivial in-plane momentum dependence for-quasi two-dimensional systems. This effect is induced purely by Coulomb interactions and not by quantum well disorder [79].

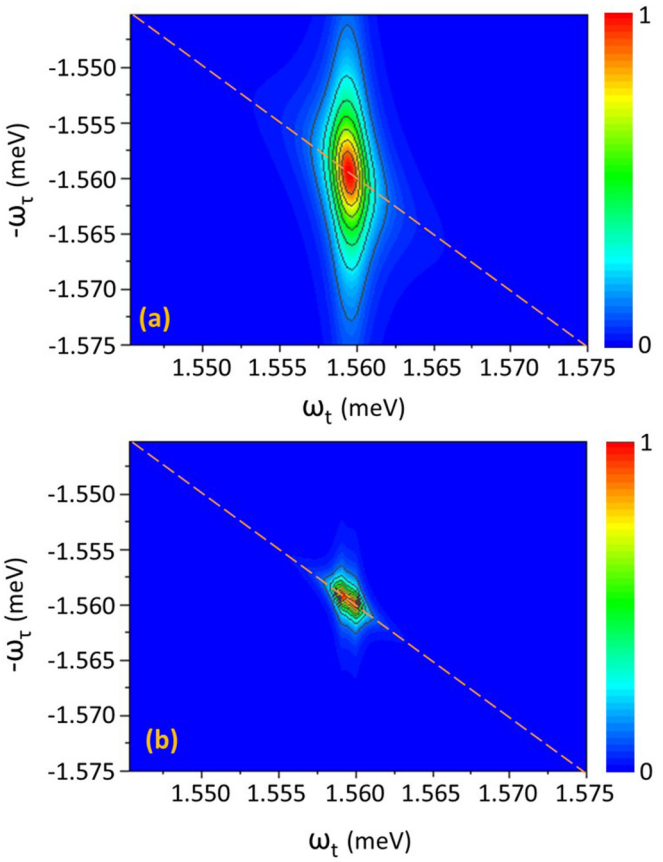

FIG. 7. (a) 2DFT spectrum of the undoped quantum well at field magnetic fields of 6 T. (b) The corresponding spectrum obtained by using the interaction functions obtained for a unit cell expanded four times in the in-plane directions.

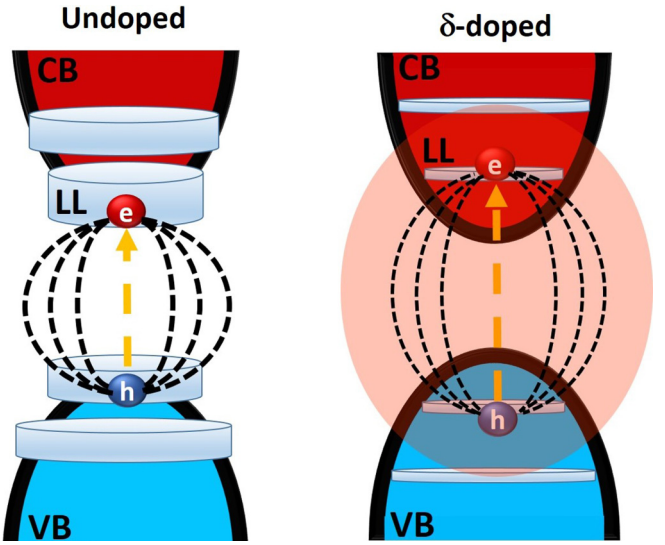

FIG. 8. Simplified schematic of the Landau levels and band structure in the undoped (left) and modulation doped (right) samples. The strong Coulomb interaction between the unscreened carriers in the undoped quantum well, depicted by the thick black arrows, leads to lifting the degeneracy of the Landau levels and coupling them to a continuum. This is depicted in a simplified manner by the broadened Landau levels for the undoped sample. In the modulation doped (δ-doped) sample the screening generated by the electron doping significantly weakens the Coulomb interactions, leaving the Landau levels degenerate. The charge screening is schematically depicted by the pink cloud, whereas the Coulomb lines are weaker and the Landau levels are discrete.

In order to test the validity of our conclusions and demonstrate the importance of the charge inhomogeneity effects, we calculate the 2DFT spectra for a unit cell artificially expanded four times in the in-plane direction. In this case, the in-plane unit cell parameter is larger than the distance between the electron and hole charge distributions. As a result, the charge inhomogeneity within the overlap of the electron and hole charge density is artificially weakened. The calculated spectra are shown in Fig. 7, and we obtain the usual line shape that does not show the elongation along ω_τ in the 2DFT spectra. This clearly indicates the origin of the peculiar lines we observe. In the doped case, the screening introduced by the dopant reduces the perturbation effect on the electron and hole. It leads to a reduced amplitude of the matrix element, which in a sense is equivalent to weakening these fluctuations.

After obtaining quantitative agreement in the undoped sample, we calculate the 2DFT LL1 and LL0 spectra for the modulation doped quantum well. Further quantitative agreement is achieved for the modulation doped sample, where the time-dependent DFT calculations reproduce well the disappearance of the elongated vertical line shapes for LL0 at 10 T. The time-dependent DFT provides illuminating insights into this seemingly counterintuitive observation. The screening generated by the free carrier weakens the effect of the fluctuations within the charge density overlap, described by the inhomogeneities of the exchange-correlation kernel. Furthermore, the shrinking of the Landau level radius with magnetic field leads to a substantial decrease of scattering probability with free electrons. The combined effect leads to the disappearance of the peculiar elongation in the ω_τ frequency direction in the 2DFT spectra and a reduction of free-carrier induced dephasing. As a result, the LL0 state reaches a homogeneous linewidth of $\sim$0.27 meV at 10 T, obtained experimentally from the cross-diagonal profile of the resonance peak in the 2DFT spectra, well in agreement with the measured dephasing time using time-integrated FWM.

Finally, we use a simple diagrammatic description in order to summarize the essential physics obtained from the time-dependent DFT calculations. In Fig. 8 we show the band structure and Landau levels for the undoped and doped quantum wells. The laser pulse promotes an electron into the Landau levels, creating a positively charged hole in the valence band. The attractive Coulomb interaction between the electron and the hole is depicted by the dashed field lines. In the undoped case the bare Coulomb interactions between the electron and hole, and the repulsive electron-electron interactions, lead to stronger Coulomb interactions, and thus the effect of the inhomogeneities within the reduced charge density overlap is stronger. These inhomogeneities within the overlap of the electron and hole charge density distributions break the translational symmetry of the in-plane charge excitations and drive the system outside the Kohn's theorem limits. As a result, the degeneracy of the Landau levels

is lifted and the Landau levels are coupled to a continuum. In the modulation doped case the Coulomb interactions are substantially weakened due to the screening provided by the electron doping. Furthermore, orbital-localization effects with increasing magnetic fields lead to an additional reduction in quasiparticle scattering. Thus, the Kohn's theorem is restored and the Landau levels remain discrete.

V. CONCLUSIONS

In this article, we demonstrate the combined effect of Coulomb interactions and extreme quantum confinement on the electronic properties of two-dimensional electron gases, such as the validity of the jellium model and Kohn's theorem. In the regime of twofold quantum confinement, namely, in the out-of-plane direction provided by the quantum well barrier and in plane by the strong magnetic fields, the charge distributions of electrons and holes become strongly localized. The charge separation leads to an overlap region that is increasingly smaller with increasing magnetic fields and eventually becomes comparable to the in-plane unit cell. At this regime the microscopic details of the charge density distribution, namely the spatial fluctuations, become significant. This leads to a breakdown of the smooth charge assumption in the jellium model and and brings the system outside the protective limit of Kohn's theorem. This breakdown is facilitated by the strong unscreened Coulomb interactions in the intrinsic sample. When the Coulomb interactions are weakened, the system returns to the usual assumption of smooth charge distribution and translation invariance along the plane.

ACKNOWLEDGMENTS

The work at USF and UAB was supported by the National Science Foundation under Grant No. DMR-1409473. The development of the experimental technique was in part supported by the US Department of Energy, Office of Basic Energy Sciences, Division of Materials Sciences and Engineering under Award No. DE-SC0012635. V.T. thanks the DOE for partial support under Grant No. DOE-DE-FG02-07ER46354. This work was performed, in part, at the Center for Integrated Nanotechnologies, a US Department of Energy, Office of Basic Energy Sciences user facility. Sandia National Laboratories is a multiprogram laboratory managed and operated by Sandia Corporation, a wholly owned subsidiary of Lockheed Martin Corporation, for the US Department of Energy's National Nuclear Security Administration under Contract No. DE-AC04-94AL85000.

[1] G. H. Wannier, Phys. Rev. **52**, 191 (1937).
[2] H. Haug and S. W. Koch, *Quantum Theory of the Optical and Electronic Properties of Semiconductors* (World Scientific, Singapore, 2009).
[3] D. C. Rogers, J. Singleton, R. J. Nicholas, C. T. Foxon, and K. Woodbridge, Phys. Rev. B **34**, 4002 (1986).
[4] L. Viña, G. E. W. Bauer, M. Potemski, J. C. Maan, E. E. Mendez, and W. I. Wang, Phys. Rev. B **41**, 10767 (1990).
[5] A. Petrou, G. Waytena, X. Liu, J. Ralston, and G. Wicks, Phys. Rev. B **34**, 7436 (1986).
[6] C. Delalande, G. Bastard, J. Orgonasi, J. A. Brum, H. W. Liu, M. Voos, G. Weimann, and W. Schlapp, Phys. Rev. Lett. **59**, 2690 (1987).
[7] F. Meseguer, J. C. Maan, and K. Ploog, Phys. Rev. B **35**, 2505(R) (1987).
[8] R. B. Laughlin, Phys. Rev. B **23**, 5632 (1981).
[9] M. Z. Hasan and C. L. Kane, Rev. Mod. Phys. **82**, 3045 (2010).
[10] A. Pinczuk, J. P. Valladares, D. Heiman, A. C. Gossard, J. H. English, C. W. Tu, L. Pfeiffer, and K. West, Phys. Rev. Lett. **61**, 2701 (1988).
[11] A. Pinczuk, S. Schmitt-Rink, G. Danan, J. P. Valladares, L. N. Pfeiffer, and K. W. West, Phys. Rev. Lett. **63**, 1633 (1989).
[12] G. Danan, A. Pinczuk, J. P. Valladares, L. N. Pfeiffer, K. W. West, and C. W. Tu, Phys. Rev. B **39**, 5512 (1989).
[13] A. Pinczuk, B. S. Dennis, D. Heiman, C. Kallin, L. Brey, C. Tejedor, S. Schmitt-Rink, L. N. Pfeiffer, and K. W. West, Phys. Rev. Lett. **68**, 3623 (1992).
[14] A. Pinczuk, B. S. Dennis, L. N. Pfeiffer, and K. West, Phys. Rev. Lett. **70**, 3983 (1993).
[15] D. Heiman, B. B. Goldberg, A. Pinczuk, C. W. Tu, A. C. Gossard, and J. H. English, Phys. Rev. Lett. **61**, 605 (1988).
[16] H. Buhmann, W. Joss, K. von Klitzing, I. V. Kukushkin, G. Martinez, A. S. Plaut, K. Ploog, and V. B. Timofeev, Phys. Rev. Lett. **65**, 1056 (1990).
[17] A. J. Turberfield, S. R. Haynes, P. A. Wright, R. A. Ford, R. G. Clark, J. F. Ryan, J. J. Harris, and C. T. Foxon, Phys. Rev. Lett. **65**, 637 (1990).
[18] B. B. Goldberg, D. Heiman, A. Pinczuk, L. Pfeiffer, and K. West, Phys. Rev. Lett. **65**, 641 (1990).
[19] B. B. Goldberg, D. Heiman, M. Dahl, A. Pinczuk, L. Pfeiffer, and K. West, Phys. Rev. B **44**, 4006 (1991).
[20] B. B. Goldberg, D. Heiman, M. J. Graf, D. A. Broido, A. Pinczuk, C. W. Tu, J. H. English, and A. C. Gossard, Phys. Rev. B **38**, 10131(R) (1988).
[21] B. B. Goldberg, D. Heiman, and A. Pinczuk, Phys. Rev. Lett. **63**, 1102 (1989).
[22] M. Dahl, D. Heiman, A. Pinczuk, B. B. Goldberg, L. N. Pfeiffer, and K. W. West, Phys. Rev. B **45**, 6957 (1992).
[23] M. A. Eriksson, A. Pinczuk, B. S. Dennis, S. H. Simon, L. N. Pfeiffer, and K. W. West, Phys. Rev. Lett. **82**, 2163 (1999).
[24] M. Kang, A. Pinczuk, B. S. Dennis, M. A. Eriksson, L. N. Pfeiffer, and K. W. West, Phys. Rev. Lett. **84**, 546 (2000).
[25] M. Kang, A. Pinczuk, B. S. Dennis, L. N. Pfeiffer, and K. W. West, Phys. Rev. Lett. **86**, 2637 (2001).
[26] C. F. Hirjibehedin, A. Pinczuk, B. S. Dennis, L. N. Pfeiffer, and K. W. West, Phys. Rev. Lett. **91**, 186802 (2003).
[27] I. Dujovne, A. Pinczuk, M. Kang, B. S. Dennis, L. N. Pfeiffer, and K. W. West, Phys. Rev. Lett. **90**, 036803 (2003).
[28] I. Dujovne, A. Pinczuk, M. Kang, B. S. Dennis, L. N. Pfeiffer, and K. W. West, Phys. Rev. Lett. **95**, 056808 (2005).
[29] Y. Gallais, T. H. Kirschenmann, I. Dujovne, C. F. Hirjibehedin, A. Pinczuk, B. S. Dennis, L. N. Pfeiffer, and K. W. West, Phys. Rev. Lett. **97**, 036804 (2006).

[30] J. G. Groshaus, I. Dujovne, Y. Gallais, C. F. Hirjibehedin, A. Pinczuk, Y.-W. Tan, H. Stormer, B. S. Dennis, L. N. Pfeiffer, and K. W. West, Phys. Rev. Lett. **100**, 046804 (2008).

[31] D. S. Chemla and J. Shah, Nature (London) **411**, 549 (2001).

[32] K. Leo, M. Wegener, J. Shah, D. S. Chemla, E. O. Göbel, T. C. Damen, S. Schmitt-Rink, and W. Schäfer, Phys. Rev. Lett. **65**, 1340 (1990).

[33] N. A. Fromer, C. Schüller, D. S. Chemla, T. V. Shahbazyan, I. E. Perakis, K. Maranowski, and A. C. Gossard, Phys. Rev. Lett. **83**, 4646 (1999).

[34] P. Kner, S. Bar-Ad, M. V. Marquezini, D. S. Chemla, R. Lövenich, and W. Schäfer, Phys. Rev. B **60**, 4731 (1999).

[35] N. A. Fromer, C. Schüller, C. W. Lai, D. S. Chemla, I. E. Perakis, D. Driscoll, and A. C. Gossard, Phys. Rev. B **66**, 205314 (2002).

[36] Y. E. Lozovik, I. V. Ovchinnikov, S. Y. Volkov, L. V. Butov, and D. S. Chemla, Phys. Rev. B **65**, 235304 (2002).

[37] N. A. Fromer, C. E. Lai, D. S. Chemla, I. E. Perakis, D. Driscoll, and A. C. Gossard, Phys. Rev. Lett. **89**, 067401 (2002).

[38] K. M. Dani, J. Tignon, M. Breit, D. S. Chemla, E. G. Kavousanaki, and I. E. Perakis, Phys. Rev. Lett. **97**, 057401 (2006).

[39] A. T. Karathanos, I. E. Perakis, N. A. Fromer, and D. S. Chemla, Phys. Rev. B **67**, 035316 (2003).

[40] K. M. Dani, I. A. Cotoros, J. Wang, J. Tignon, D. S. Chemla, E. G. Kavousanaki, and I. E. Perakis, Phys. Rev. B **78**, 041301 (2008).

[41] R. A. Kaindl, D. Hägele, M. A. Carnahan, and D. S. Chemla, Phys. Rev. B **79**, 045320 (2009).

[42] D. Karaiskaj, A. D. Bristow, L. Yang, X. Dai, R. P. Mirin, S. Mukamel, and S. T. Cundiff, Phys. Rev. Lett. **104**, 117401 (2010).

[43] K. W. Stone, K. Gundogdu, D. B. Turner, X. Li, S. T. Cundiff, and K. A. Nelson, Science **324**, 1169 (2009).

[44] D. Turner and K. Nelson, Nature (London) **466**, 1089 (2010).

[45] P. Dey, J. Paul, N. Glikin, Z. D. Kovalyuk, Z. R. Kudrynskyi, A. H. Romero, and D. Karaiskaj, Phys. Rev. B **89**, 125128 (2014).

[46] P. Dey, J. Paul, G. Moody, C. E. Stevens, N. Glikin, Z. D. Kovalyuk, Z. R. Kudrynskyi, A. H. Romero, A. Cantarero, D. J. Hilton, and D. Karaiskaj, J. Chem. Phys. **142**, 212422 (2015).

[47] J. Paul, C. E. Stevens, C. Liu, P. Dey, C. McIntyre, V. Turkowski, J. L. Reno, D. J. Hilton, and D. Karaiskaj, Phys. Rev. Lett. **116**, 157401 (2016).

[48] J. Bylsma, P. Dey, J. Paul, S. Hoogland, E. H. Sargent, J. M. Luther, M. C. Beard, and D. Karaiskaj, Phys. Rev. B **86**, 125322 (2012).

[49] P. Dey, J. Paul, J. Bylsma, S. Deminico, and D. Karaiskaj, Rev. Sci. Instrum. **84**, 023107 (2013).

[50] A. D. Bristow, D. Karaiskaj, X. Dai, T. Zhang, C. Carlsson, K. R. Hagen, R. Jimenez, and S. T. Cundiff, Rev. Sci. Instrum. **80**, 073108 (2009).

[51] C. N. Borca, T. Zhang, X. Li, and S. T. Cundiff, Chem. Phys. Lett. **416**, 311 (2005).

[52] T. Zhang, I. Kuznetsova, T. Meier, X. Li, R. P. Mirin, P. Thomas, and S. T. Cundiff, Proc. Natl. Acad. Sci. USA **104**, 14227 (2007).

[53] V. Turkowski and C. A. Ullrich, Phys. Rev. B **77**, 075204 (2008).

[54] V. Turkowski, A. Leonardo, and C. A. Ullrich, Phys. Rev. B **79**, 233201 (2009).

[55] V. Turkowski and M. N. Leuenberger, Phys. Rev. B **89**, 075309 (2014).

[56] A. Ramirez-Torres, V. Turkowski, and T. S. Rahman, Phys. Rev. B **90**, 085419 (2014).

[57] W. Kohn, Phys. Rev. **123**, 1242 (1961).

[58] T. Maag, A. Bayer, S. Baierl, M. Hohenleutner, T. Korn, C. Schüller, D. Schuh, D. Bougeard, C. Lange, R. Huber, M. Mootz, J. E. Sipe, S. W. Koch, and M. Kira, Nat. Phys. **12**, 119 (2016).

[59] M. Mittendorff, F. Wendler, E. Malic, A. Knorr, M. Orlita, M. Potemski, C. Berger, W. A. de Heer, H. Schneider, M. Helm, and S. Winnerl, Nat. Phys. **11**, 75 (2015).

[60] X. Li, T. Zhang, C. N. Borca, and S. T. Cundiff, Phys. Rev. Lett. **96**, 057406 (2006).

[61] S. T. Cundiff, Opt. Express **16**, 4639 (2008).

[62] S. Mukamel, *Principles of Nonlinear Optical Spectroscopy* (Oxford University Press, Cambridge, 1995).

[63] J. Paul, P. Dey, T. Tokumoto, J. L. Reno, D. J. Hilton, and D. Karaiskaj, J. Chem. Phys. **141**, 134505 (2014).

[64] J. C. Maan, G. Belle, A. Fasolino, M. Altarelli, and K. Ploog, Phys. Rev. B **30**, 2253 (1984).

[65] A. H. MacDonald and D. S. Ritchie, Phys. Rev. B **33**, 8336 (1986).

[66] S.-R. Eric Yang and L. J. Sham, Phys. Rev. Lett. **58**, 2598 (1987).

[67] G. E. W. Bauer and T. Ando, Phys. Rev. B **37**, 3130 (1988).

[68] J. B. Stark, W. H. Knox, D. S. Chemla, W. Schäfer, S. Schmitt-Rink, and C. Stafford, Phys. Rev. Lett. **65**, 3033 (1990).

[69] Y. Iimura, Y. Segawa, G. E. W. Bauer, M. M. Lin, Y. Aoyagi, and S. Namba, Phys. Rev. B **42**, 1478 (1990).

[70] M. E. Karadimitriou, E. G. Kavousanaki, I. E. Perakis, and K. M. Dani, Phys. Rev. B **82**, 165313 (2010).

[71] M. E. Karadimitriou, E. G. Kavousanaki, K. M. Dani, N. A. Fromer, and I. E. Perakis, J. Phys. Chem. B **115**, 5634 (2011).

[72] C. Kallin and B. I. Halperin, Phys. Rev. B **30**, 5655 (1984).

[73] C. Kallin and B. I. Halperin, Phys. Rev. B **31**, 3635 (1985).

[74] A. Delteil, A. Vasanelli, Y. Todorov, C. Feuillet Palma, M. R. St-Jean, G. Beaudoin, I. Sagnes, and C. Sirtori, Phys. Rev. Lett. **109**, 246808 (2012).

[75] L. D. Landau and L. M. Lifshitz, *Quantum Mechanics, Third Edition: Non-Relativistic Theory (Vol. 3)* (Butterworth-Heinemann, Oxford, 1981).

[76] See Supplemental Material at http://link.aps.org/supplemental/10.1103/PhysRevB.95.245314 for details on the calculations using time-dependent density functional theory and the experimental technique, which includes Refs. [35,42–44,46–48,50,53–56,63].

[77] C. M. Hu, E. Batke, K. Köhler, and P. Ganser, Phys. Rev. Lett. **75**, 918 (1995).

[78] C. M. Hu, E. Batke, K. Köhler, and P. Ganser, Phys. Rev. Lett. **76**, 1904 (1996).

[79] Z. Schlesinger, W. I. Wang, and A. H. MacDonald, Phys. Rev. Lett. **58**, 73 (1987).